nature catalysis

ARTICLES

https://doi.org/10.1038/s41929-020-00533-6

Check for updates

Shape-selective C–H activation of aromatics to biarylic compounds using molecular palladium in zeolites

Jannick Vercammen[1], Massimo Bocus[2], Sam Neale[2], Aram Bugaev[3], Patrick Tomkins[1], Julianna Hajek[2], Sam Van Minnebruggen[1], Alexander Soldatov[3], Andraž Krajnc[4], Gregor Mali[4], Véronique Van Speybroeck[2]✉ and Dirk E. De Vos[1]✉

The selective activation of inert C–H bonds has emerged as a promising tool for avoiding the use of wasteful traditional coupling reactions. Oxidative coupling of simple aromatics allows for a cost-effective synthesis of biaryls. However, utilization of this technology is severely hampered by poor regioselectivity and by the limited stability of state-of-the-art homogeneous Pd catalysts. Here, we show that confinement of cationic Pd in the pores of a zeolite allows for the shape-selective C–H activation of simple aromatics without a functional handle or electronic bias. For instance, out of six possible isomers, 4,4′-bitolyl is produced with high shape selectivity (80%) in oxidative toluene coupling on Pd-Beta. Not only is a robust, heterogeneous catalytic system obtained, but this concept is also set to control the selectivity in transition-metal-catalysed arene C–H activation through spatial confinement in zeolite pores.

Biarylic bonds are an important structural motif in numerous organic chemicals. Currently, the industrial production of biaryl compounds relies on traditional coupling reactions (Suzuki, Ullmann and so on) which use pre-activated arenes (for example, aryl halides and arylboronic acids)[1]. The high cost of these intermediates and the associated reaction waste generated usually direct the application of these coupling reactions towards making high-end, speciality chemicals. Especially in the polymer industry there has been a growing demand for biarylic monomers because of their superior chemical and physical stability, and their favourable health and safety profiles[2–4].

The direct functionalization of unreactive C–H bonds via transition-metal-mediated C–H activation has emerged as a promising alternative to traditional multi-step approaches[1]. C–H/C–H arene–arene couplings can in principle be used for the direct synthesis of biaryls from simple arenes with, for example, Pd carboxylates as the catalysts[5–10]. If O_2 is used as the oxidant, water is the only by-product[11]. Unfortunately, the multitude of C–H bonds present in organic reactants and the poor differentiation between them often result in poor regioselectivity. Consequently, reactions with simple arenes (for example toluene) lead to useless mixtures of many isomers[12]. Selectivity for the *ortho* position can be achieved if the existing substituent exerts a directing effect, as is typical for ketone groups, carbamates, amides and so on[13]. Complex schemes must be adopted to achieve some *meta* selectivity, for example by installing pendant groups on the ligand of the catalytic complex[14]. Finally, *para* selectivity realized recently *via* pre-functionalization with highly electrophilic radicals[15,16] and by installing extreme steric bulk on the aromatic reactant, for example by using pivaloyl-derivatized reactants[17]. Clearly, these complex reactants are quite far from the simple, monosubstituted aromatics that one would desire to functionalize functionalizing in a regioselective way.

A so-far unexplored option is to implement the molecular mechanisms of transition-metal-catalysed C–H activation in the shape-selective confinement of a porous material like a zeolite. Zeolites are microporous, crystalline aluminosilicates; they are applied on a large scale in industrial reactions because of their excellent activity and stability, along with their low cost. The molecular dimensions and shape of the pores may direct the selectivity to particular products via the imposed steric constraints[18]. This shape selectivity has been extensively studied for acid-catalysed reactions. However, zeolites have so far not been used to create a shape-selective environment around molecular catalysts that activate C–H bonds of arenes to form more complex organics[19].

Here we demonstrate that Pd(II) catalysts, site-isolated in the framework of zeolite Beta or some other 12-membered-ring (12-MR) zeolites, uniquely allow oxidative coupling of toluene and other monosubstituted aromatics to biaryls, with exceptional selectivity for the *p*,*p*′-dimer.

Results

Pd catalysts at work in zeolite hosts. The most active homogeneous catalysts for the oxidative coupling of arenes generally comprise a palladium salt, a strongly acidic additive, for example, *p*-toluenesulfonic acid (TsOH) or trifluoroacetic acid (TFAH) and acetic acid (AcOH)[5–10]. When applying such homogeneous catalysts to toluene (Fig. 1), an unbiased regioisomer distribution is obtained, with all C–H bonds being activated by Pd to a similar extent (Supplementary Figs. 2 and 3; Supplementary Table 1). Furthermore, side products were identified, resulting from oxygenation, from benzylic coupling and, especially at higher conversions, from consecutive coupling to trimers (4.8 mol% trimer at 8.0% toluene conversion). We first set out to replace the strongly acidic

[1]Centre for Membrane Separations, Adsorption, Catalysis, and Spectroscopy for Sustainable Solutions (cMACS), KU Leuven, Leuven, Belgium. [2]Center for Molecular Modeling (CMM), Ghent University, Zwijnaarde, Belgium. [3]The Smart Materials Research Institute, Southern Federal University, Rostov-on-Don, Russia. [4]Department of Inorganic Chemistry and Technology, National Institute of Chemistry, Ljubljana, Slovenia. ✉e-mail: Veronique.vanspeybroeck@ugent.be; dirk.devos@kuleuven.be

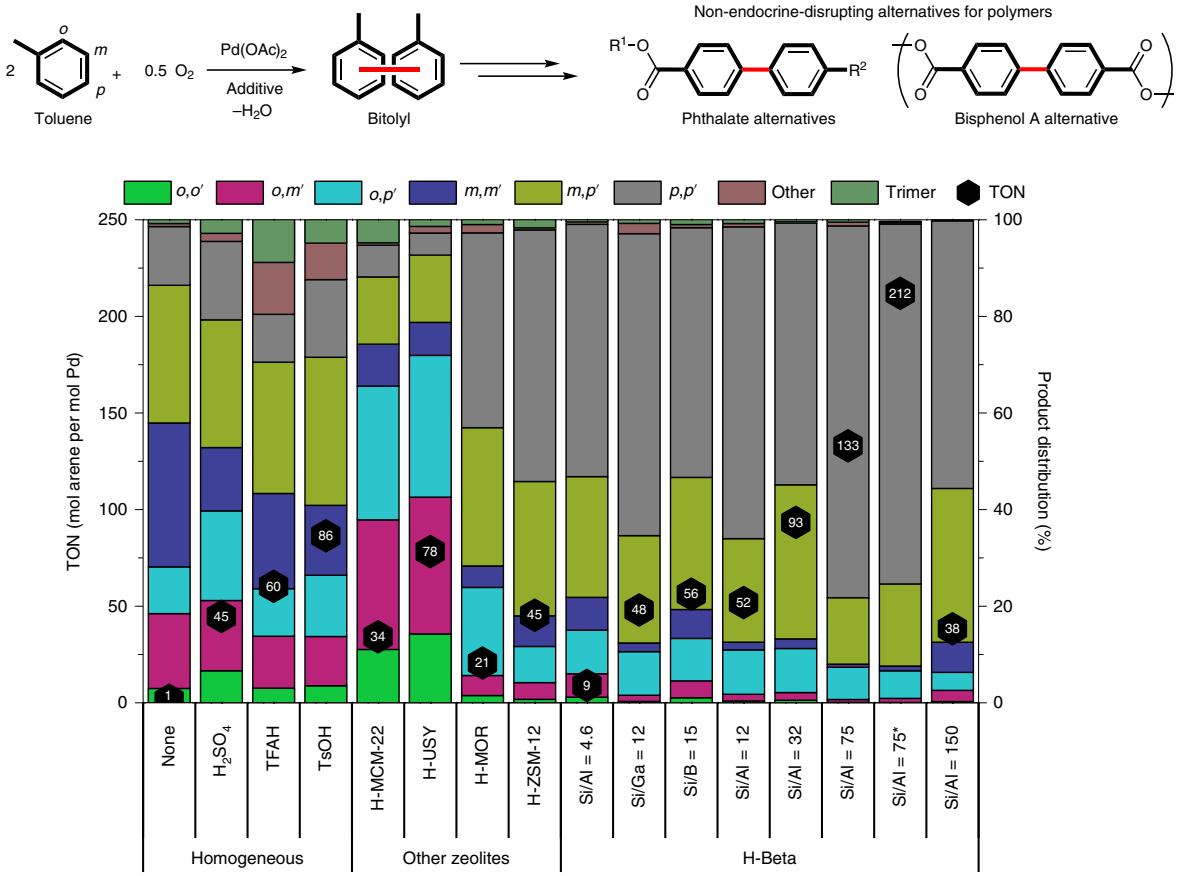

Fig. 1 | Oxidative coupling of toluene with different additives. Reaction conditions: 15 µmol $Pd(OAc)_2$, 2 ml toluene, 90 °C, 16 bar O_2, 16 h. Homogeneous reactions employed 0.3 mmol of the additive and 1 ml AcOH, while reaction with zeolites used 50 mg at Si/Al < 50 and 100 mg at Si/Al > 50. *AcOH (200 equiv. to Pd) was added.

additives with acid zeolites, initially without acetic acid, to simplify the reaction mixture. At equal loadings of $Pd(OAc)_2$, bitolyl formation with the addition of acid zeolites not only surpassed that with any other solid acid tested, but occasionally even the homogeneous catalyst tested under the same conditions (Fig. 1). Large-pore zeolites (that is with 12-MRs) were required to offer sufficient space for toluene and other substituted arenes to react; medium-pore zeolites such as H-ZSM-5 were only effective for the oxidative coupling of benzene. To our delight, zeolites not only with three-dimensional pores (H-Beta) but also with one-dimensional pores (H-MOR, H-ZSM-12 and so on), which are more susceptible to diffusion restrictions, could be used to boost the catalytic performance of Pd in this reaction.

The most remarkable feature of this disclosure is the regioselectivity in the biaryl product if zeolites are applied. Out of the six possible bitolyl regiomers, zeolites containing only 12-MR channels and no large cavities (H-MOR, H-ZSM-12, H-Beta) were highly selective for *para*-substituted products. In H-Beta, the combined selectivity for all products with at least one *para* substituent reaches 97% in H-Beta and with a selectivity of 77% for *p*,*p*′-bitolyl, compared to only 59 and 16% respectively for a homogeneous catalyst with TsOH. Zeolites with large cages (H-USY, H-MCM-22) showed a high combined selectivity for products with at least one *ortho* substituent (72% for H-USY compared to 28% for TsOH). Furthermore, side reactions, such as coupling at the benzylic position or oxygenation reactions, were suppressed in 12-MR zeolites like H-Beta. On MCM-22, known for its surface activity[20], some trimer formation was observed, but such consecutive coupling at higher conversions was inhibited in the microporous environment of the other tested 12-MR zeolites.

Towards high activity and selectivity. In view of the intriguing shape selectivity for a double C–H activation at the *para* position combined with the exceptional activity of Pd-loaded H-Beta, we decided to investigate this system further (Supplementary Figs. 4–11). Addition of small amounts of acetic acid (1–500 equiv. to Pd) further boosted the performance to a turnover number (TON) of 212 or a yield of 16.8% while maintaining an identical product distribution (Supplementary Fig. 12). High zeolite Si/Al ratios were required for obtaining higher TON values (Fig. 1). This is likely unrelated to acid strength since similar results were obtained with Ga- and B-substituted Beta. Rather, the beneficial effect of the high Si/Al ratio seems related to the more hydrophobic properties of such a zeolite (Fig. 1). A decline in regioselectivity during the reaction was observed at a Si/Al ratio of 32 (Supplementary Fig. 6) while the regioselectivity remained constant and even improved initially at the higher Si/Al ratio of 75 (Fig. 4b). This was attributed to a poisoning effect of the formed water[21], which was subsequently confirmed by spiking reactions with 100 µl of water (370 equiv. to Pd): here the TON was decreased drastically from 93 to 2 for a Si/Al of 32, but the TON decreased only slightly, from 133 to 96, for the more hydrophobic zeolite Beta with a Si/Al of 75. The excellent catalytic stability of H-Beta is further highlighted by a doubling of the TON from 212 to 422 (bitolyl yield 34%) upon increasing the reaction temperature from 90 to 110 °C (Fig. 2). High TONs were obtained at O_2 pressures of 16 bar or more; however, the addition

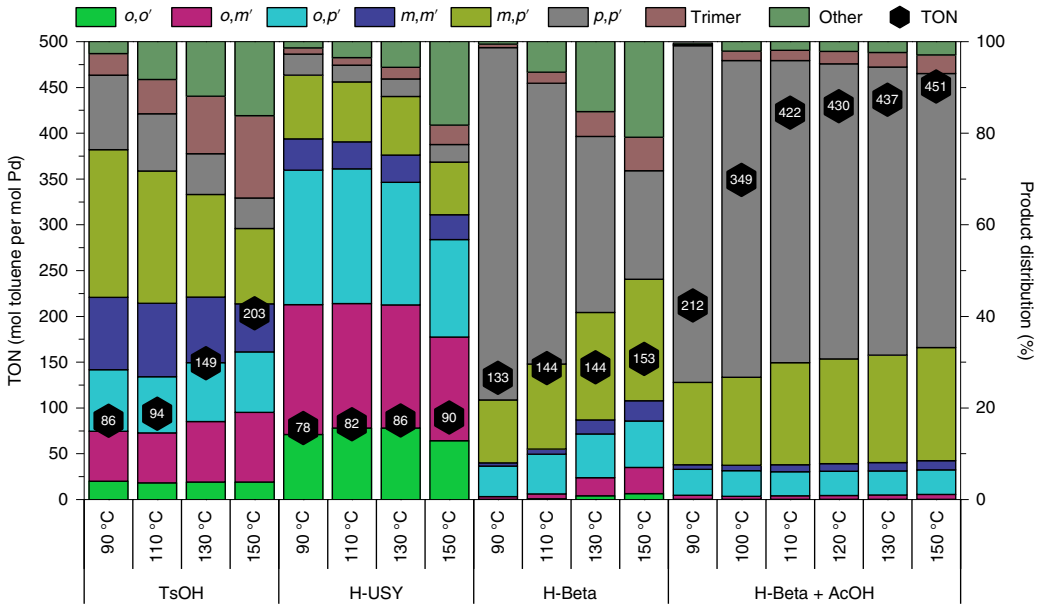

Fig. 2 | Variation of the reaction temperature in the oxidative coupling of toluene. Reaction conditions: 15 µmol $Pd(OAc)_2$, 2 ml toluene, 16 bar O_2, 16 h. Following amounts were employed: TsOH (0.3 mmol) and 1 ml AcOH, H-USY (Si/Al = 40, 50 mg), H-Beta (Si/Al = 75, 100 mg), H-Beta + AcOH (200 equiv. AcOH to Pd).

of $Fe(OTf)_3$ also allows the zeolite Beta system to reach significant TONs under only 1 bar of O_2 (see Supplementary Table 2).

Nature of the active site. The catalytic species Pd-Beta, formed upon loading the H-Beta zeolite with $Pd(OAc)_2$, was characterized in detail (Fig. 3). X-ray absorption near edge structure (XANES) spectra are consistent with Pd(II) being surrounded by four neighbouring oxygen atoms in a square planar coordination; Pd prevails in the +2 state, while the contribution of Pd(0) nanoparticles is only minor (Supplementary Figs. 14 and 15, Supplementary Table 3). When the loading is performed in toluene, the spectral changes suggest that one of these oxygen atoms may be replaced by a nearby toluene molecule (Supplementary Fig. 16). Extended X-ray absorption fine structure (EXAFS) spectra were successfully modelled with mononuclear Pd(II) with four oxygen neighbours; although there could be a small contribution from Pd(0) nanoparticles, the presence of di- or trinuclear Pd, as in the precursor $Pd(OAc)_2$, can be excluded. Again, upon loading in toluene, the best fit is obtained with three oxygen atoms from the zeolite and an acetate, together with a nearby toluene (Fig. 3a; Supplementary Fig. 17; Supplementary Tables 4–6). Solid-state ^{13}C magic-angle spinning NMR of the acid zeolite Beta loaded with ^{13}C-enriched $Pd(OAc)_2$ proved that one acetate out of the two reacts to form acetic acid, moving freely in the pores, while the second acetate remains immobilized at a Pd centre (Supplementary Fig. 21). The mutual proximity of acetate ligands was probed using 2D ^{13}C–^{13}C spin-diffusion experiments and 1D ^{13}C double-quantum-filtered experiments (Fig. 3; Supplementary Figs. 22 and 23), which proved that the individual acetates are spatially isolated from other acetate ligands. This combined information points to a molecular Pd(II) species that receives one charge compensation from the framework and one from a pendant acetate ligand. However, it does not rule out the possibility that a fraction of Pd is compensated by two anionic zeolite charges.

Such catalytic species can be formed in zeolite Beta, either in situ in toluene or prior to the reaction (Supplementary Fig. 13). The zeolite amount was varied at a fixed amount of Pd; the reaction rate increased linearly until an Al/Pd ratio of 1 was reached. This supports the single charge compensation of each Pd centre by the zeolite (Fig. 4a). The crucial presence of the acetate ligand was shown by the absence of any reaction if a Pd(II)-zeolite was prepared via classical ion-exchange with $Pd(NH_3)_4^{2+}$ and subsequent calcination (Supplementary Fig. 24), where the catalytic activity could only be restored by the addition of acetic acid. Palladium is strongly bound to the framework, as was shown by a successful filtration test which demonstrated a fully heterogeneous Pd-zeolite catalyst (Fig. 4b; Supplementary Figs. 25 and 26; Supplementary Table 7).

Producing useful biarylic monomers. The methodology could easily be expanded to the oxidative coupling of other simple arenes of interest in polymer chemistry. Oxidative coupling of anisole could lead to an alternative synthetic strategy for 4,4′-dihydroxybiphenyl, which is not only a starting material for heat-resistant materials but also a replacement for the disputed bisphenol A-derived polycarbonates[22,23]. A high activity (TON of 197) and a selectivity of 77% for *p*,*p*′-bianisyl were obtained in the oxidative homocoupling of anisole with H-Beta (Fig. 5a). While the homogeneous reaction with TsOH formed up to 56% of bisanisyl F (bis(anisyl)methane), which was due to the consecutive hydrolysis of anisole, oxidation of the formed methanol to formaldehyde and condensation reaction with anisole, only 4% of bisanisyl F was formed with H-Beta. Lastly, *p*,*p*′-bianisyl selectively precipitated from the reaction mixture upon cooling, not only simplifying the work-up but also yielding high-purity crystals (Supplementary Figs. 30 and 31). The regioselective coupling also applies to disubstituted arenes like *o*-xylene, from which the desired 3,3′,4,4′-tetramethylbiphenyl was obtained in 90% overall selectivity (Fig. 5b). This tetramethyl-substituted compound is a direct precursor of 3,3′,4,4′-biphenyldicarboxylic acid, from which high value polyimide can be produced.

Density functional theory calculations. To support the experimental observations and to obtain in-depth mechanistic information, a full catalytic cycle was proposed and calculated by means of a combination of first-principles static and molecular dynamics-based dispersion-corrected density functional theory (DFT) calculations. The first-principles molecular dynamics (MD) calculations were

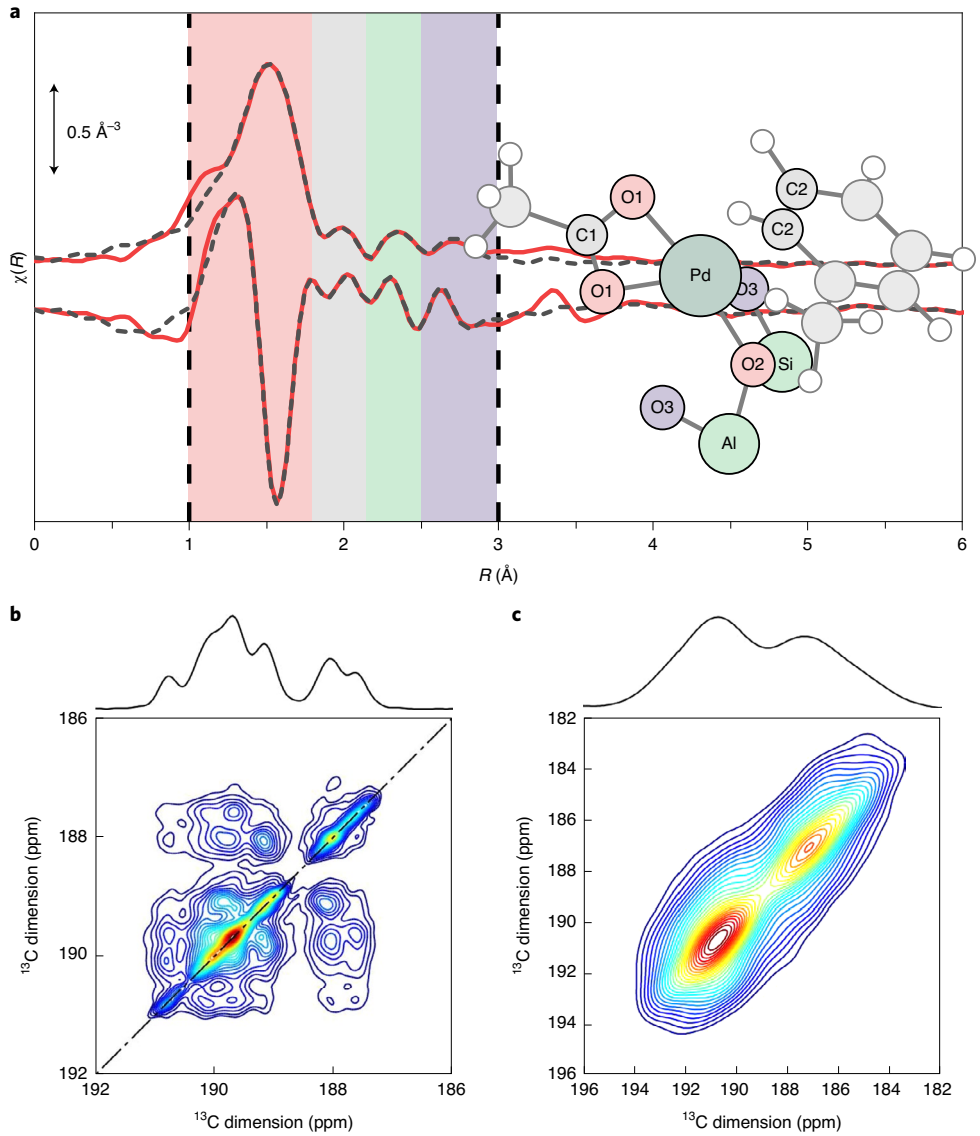

Fig. 3 | Spectroscopic characterization of Pd-loaded zeolite Beta. a, Experimental (red) and fitted (dashed grey) EXAFS spectra for Pd-Beta, pre-loaded in toluene. For the fit, the theoretically proposed intermediate **V** was used (Fig. 6b). The different background colours highlight the region with the major contribution from the atoms of the corresponding colour. **b**,**c**, 2D ^{13}C–^{13}C spin-diffusion magic-angle spinning NMR spectra of the ^{13}C-enriched $Pd(OAc)_2$ (**b**) and Pd-Beta (**c**). The absence of cross-peaks in the latter spectrum proves that the acetate ligands are spatially isolated.

employed to explore the flexible behaviour of the active catalytic site when docked to the zeolite in various stages of catalysis at realistic temperatures and toluene loadings, whereas the static DFT calculations afforded adsorption free energies and allowed for the construction of regiodivergent reaction profiles to explore the origin of shape selectivity in the reaction. The proposed catalytic cycle for the homocoupling reaction of toluene in H-Beta is reported in Fig. 6a, whereas the associated free energy profile is shown in Fig. 6b.

The catalytic reaction begins with the adsorption of $Pd(OAc)_2$ into the zeolite framework, where, relative to the empty H-Beta and the isolated $Pd(OAc)_2$, the adsorption free energy is favourable and amounts to −75 kJ mol^{-1} (species **II**) at 363 K (Fig. 6b). Subsequently, the actual docking can take place as described experimentally to release AcOH and afford Pd(OAc) species **III** (−80 kJ mol^{-1}). This is mildly exergonic with respect to the preceding intermediate **II**, with a decrease in free energy of 5 kJ mol^{-1}. This proposed mechanism of docking to form **III** is fully supported by ^{13}C NMR measurements (vide supra, Fig. 3). The docked Pd species **III** then acts as the initial species in the catalytic cycle and, based on our calculations, we propose that the reaction proceeds through four elementary reaction steps (Fig. 6). After the first toluene molecule has been adsorbed on the zeolite with a favourable free energy gain of 37 kJ mol^{-1}, C–H activation takes place through a concerted metallation–deprotonation mechanism (CMD, Step 1 in Fig. 6), a pathway that has been well-studied in the literature[24]. First, the toluene must enter into the coordination sphere of Pd, substituting one of the zeolite oxygens to afford the η^2-(tolyl)Pd species **V** (−122 kJ mol^{-1}). The presence of **V** as a key reaction intermediate is in good agreement with the X-ray absorption spectroscopy (XAS) measurements of the catalyst pre-loaded with toluene (Fig. 3). Then, CMD can take place, where the calculated activation energies indicate that the reaction involving the *para* carbon is the most accessible, since the barrier amounts to 91 kJ mol^{-1} versus 101 kJ mol^{-1} and 103 kJ mol^{-1} for activation at the *meta* and *ortho* positions respectively (Supplementary Fig. 40). This suggests that the large overall 97% *para* selectivity observed experimentally is mainly governed by the kinetics of this initial

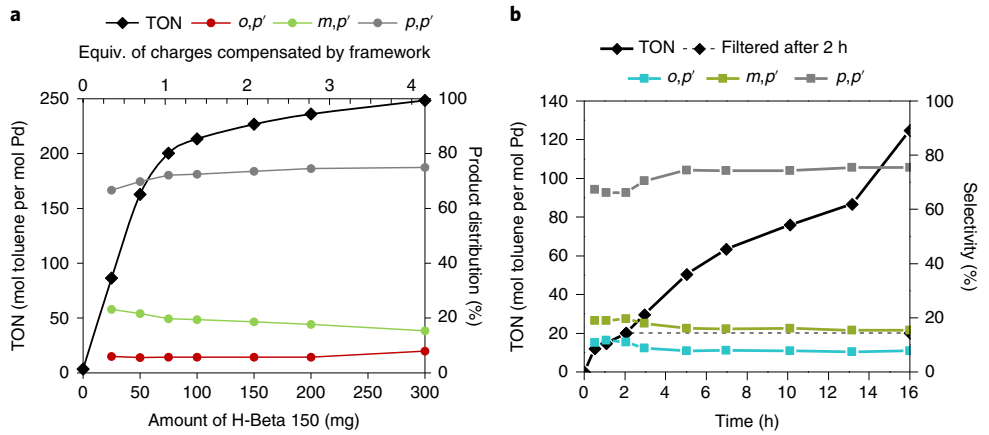

Fig. 4 | Variation of the amount of H-Beta, kinetics and filtration test. a, Variation of the amount of H-Beta (Si/Al = 75) in the oxidative coupling of toluene (2 ml) with 3 mmol AcOH added. Reaction conditions: 15 μmol $Pd(OAc)_2$, 90 °C, 16 bar O_2, 16 h. **b**, Time profile and filtration test for the oxidative coupling of toluene with H-Beta (100 mg, Si/Al = 75) without additional AcOH. After 2 h of reaction, the solids were removed by filtration and the filtrate was reacted further with fresh H-Beta (Si/Al = 75, 100 mg) for 14 h (dashed line; see Supplementary Figs. 26 and 27 for detailed description). Reaction conditions: 15 μmol $Pd(OAc)_2$, 2 ml toluene, 90 °C, 16 bar O_2.

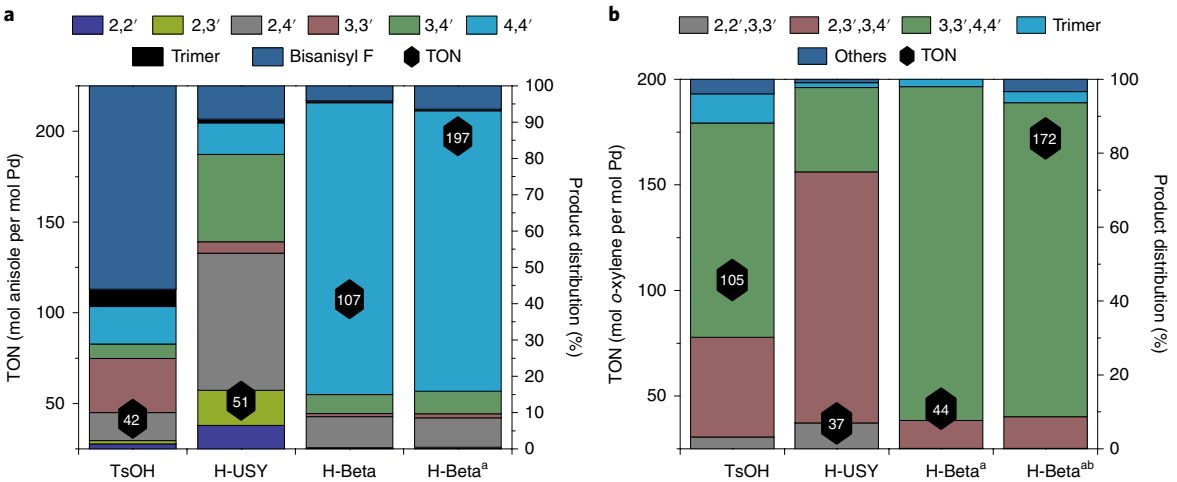

Fig. 5 | Substrate scope. a,**b**, Oxidative coupling of anisole (**a**) and *o*-xylene (**b**). Reaction conditions: 15 μmol $Pd(OAc)_2$, 2 ml arene, 90 °C, 16 bar O_2, 16 h. Following amounts were employed: TsOH (0.3 mmol) and 1 ml AcOH, H-USY (Si/Al = 40, 50 mg), H-Beta (Si/Al = 75, 100 mg). [a]AcOH added, 3 mmol. [b]Reaction temperature, 110 °C.

CMD step. It might be noticed that the *para* product has a higher energy than the others; this is caused by the methyl group directly pointing toward the zeolite walls and creating some short contacts (Supplementary Fig. 41). Further support for *para* activation was gained through an MD simulation of the reactant state, in which a predominant interaction between Pd and the toluene *para* carbon was observed (Supplementary Figs. 42–44).

After the first CMD step, we propose further C–C coupling to occur through a migratory insertion reaction (MI, Step 2 in Fig. 6, and Supplementary Figs. 45–49)[25,26]. The calculated reaction barriers for this process are relatively low (68 kJ mol^{-1} for *m*,*p*′-selectivity, 69 kJ mol^{-1} for *p*,*p*′-selectivity and 89 kJ mol^{-1} for *o*,*p*′-selectivity). To test the validity of the proposed MI mechanism further, we computed an alternative second CMD mechanism. The resulting barriers for such processes were much higher (with $\Delta G^{\ddagger} = 187$ kJ mol^{-1} for *p*,*p*′-selectivity, Supplementary Fig. 51 and Supplementary Tables 14 and 15), thus giving further support to the MI mechanism.

Moreover, experimental kinetic studies revealed a first-order rate dependence in Pd (Supplementary Fig. 36), thus further supporting the proposed MI mechanism as the favoured means of C–C coupling over a bimetallic transmetallation process. While the MI barrier difference between *m*,*p*′ and *p*,*p*′ is small (with $\Delta\Delta G^{\ddagger} = 1$ kJ mol^{-1} for the regiodivergent analogues of **TS(VII–VIII)**), the *o*,*p*′ activation energy is much higher, which arises from the increased steric clashing between the methyl group and the zeolite pore (Supplementary Fig. 49). The calculations thus suggest that the predominant overall *para* selectivity is primarily dictated by the first CMD step, while more subtle effects are at play in the rest of the catalytic cycle to afford the overall 77% yield for *p*,*p*′-bitolyl (Supplementary Fig. 47).

Subsequently, from **VIII**, the transfer of a hydrogen atom from the C–C coupled bitolyl moiety to Pd needs to take place. However, the lack of an available base does not allow for a direct reductive deprotonation, while the *anti*-configuration of Pd and the hydrogen prevent a β-hydride elimination[26,27]. We thus propose that in Step 3 a hydrogen-transfer process from the resulting C–C coupled cyclohexadienyl adduct **VIII** to the Pd centre can take place, facilitated by AcOH itself. However, accurate characterization of the corresponding transition states proved challenging, and so explicit

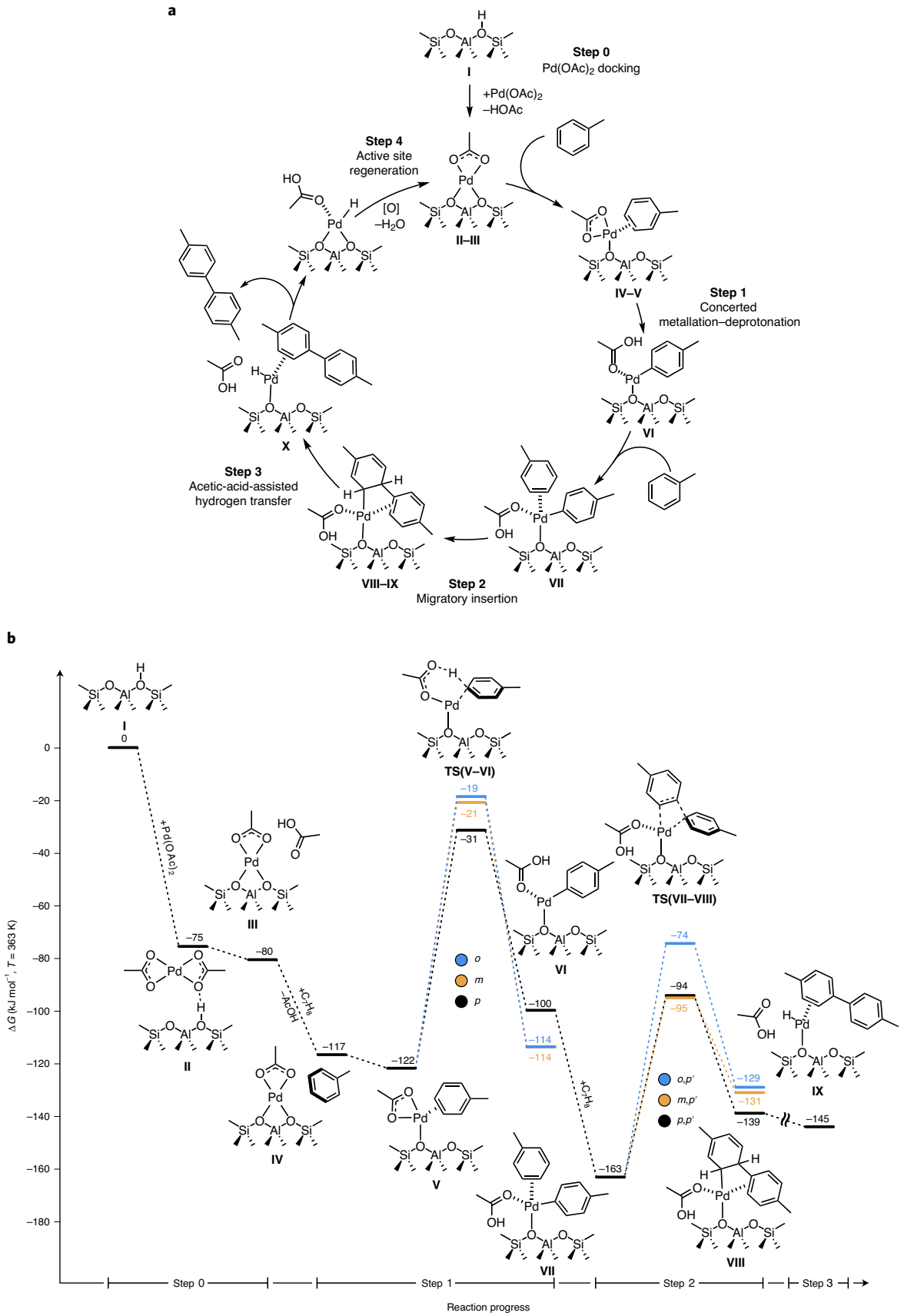

Fig. 6 | Proposed catalytic cycle for the oxidative coupling of toluene using H-Beta. a, Reaction scheme. **b**, Free energy profile of the proposed mechanism for the oxidative coupling of toluene. The profile (kJ mol^{-1}) was computed at the B3LYP-D3//PBE-D3 level of theory at 363 K. The schematic representations of the intermediates and transition states are related to the mechanism leading to the *p,p′*-bitolyl product. Enthalpic and entropic contributions to the free energy are reported in Supplementary Tables 10–15.

transition-state energies are not reported in Fig. 6b (Supplementary Fig. 50). The eventually obtained Pd hydride **IX** (−145 kJ mol^{-1}) was found to be a stable energy minimum in the free energy reaction cycle. Finally, from **IX**, active site regeneration (Step 4) is proposed to take place via O_2 insertion. Characterization of this process was carried out using a 5T cluster model to efficiently compute the spin-forbidden nature of the mechanism, as previously identified by Stahl and collaborators[28,29]. These calculations revealed that hydrogen atom abstraction (HAA) is favoured to form the resulting Pd–OOH species and ultimately release H_2O_2 (Supplementary Figs. 52 and 53)

Conclusions

We report the development of a strategy for controlling the regioselectivity in the C–H functionalization of aromatics without a functional handle. The elusive *para* selectivity is obtained through a non-traditional shape selectivity in which exchanged cationic palladium in zeolites is utilized, rather than the acidic sites of zeolites. The technology grants access to a novel range of monomers for advanced polymers; the methodology also provides a paradigm for introducing shape selectivity in the transition-metal-catalysed C–H activation of arenes.

Methods

Reaction procedure. Generally, toluene (2.00 ml, 18.88 mmol, Acros), acetic acid (172 µl, 0.3 mmol, Acros) and *n*-decane (50.0 µl, internal standard) were added to $Pd(OAc)_2$ (3.37 mg, 0.015 mmol, Acros) and H-Beta (100.0 mg, Si/Al = 75, Süd-Chemie) in a 3 ml glass liner. Homogeneous reactions were performed with 0.3 mmol of the additive and 1 ml of acetic acid, while reactions with zeolites employed 50 mg of the solid without acetic acid. Zeolites with a Si/Al ratio above 50 employed 100 mg of the solid. The liner was sealed in a homemade, stainless steel autoclave (Supplementary Fig. 1), and purged five times with pure O_2 and subsequently pressurized with pure O_2 to 16 bar. The reactor was placed in a pre-heated four-well aluminium block. The internal temperature dependence was calibrated beforehand, and the set temperature of the heating block was adjusted to obtain 90 °C internally.

After 16 h, the reactor was cooled and the zeolite was separated from the reaction mixture via centrifugation. The reaction mixture was analysed by GC-FID. When anisole was used as the aromatic reagent, the 4,4′-bianisyl product precipitated from the reaction medium upon cooling. Therefore, this mixture was extracted with $CHCl_3$ (20 ml) before GC-FID analysis to fully solubilize all products. In accordance with literature reports, the TON is defined as TON = 2 × mol biaryl / mol Pd.

Each reactor had an intentional weak spot at the capillaries on top of the reactor which functioned as a burst disc. Note: a thorough safety assessment must be made before applying such hazardous conditions and these reactions should only be performed using proper equipment that ensures safe handling at all times.

Reaction analysis. Reaction mixtures were analysed quantitatively using a Shimadzu GC-2014 equipped with a CP-SIL 5 CB column (Agilent, 100% PDMS, 60 m, 0.25 µm film thickness, 0.32 mm i.d.). Samples of 1 µl were injected automatically using an AOC-20s autosampler and AOC-20i auto-injector aided by the GCsolution software bundle (version 2.44.00). Products were identified using an Agilent 6890 gas chromatograph equipped with an HP-1 MS column and coupled to a 5973 MSD mass spectrometer or by comparison with commercially obtained or synthesized reference samples. ^{1}H NMR spectra of liquid samples were recorded using a Bruker Avance III HD 400 console at 400 MHz, equipped with a 5 mm PABBO BB/^{19}F–^{1}H/D probe and the data were analysed using the MestReNova 12.0.2 software package.

Pre-loading. Zeolites can be pre-loaded with $Pd(OAc)_2$ prior to the reaction by contacting the solid with an appropriate amount of $Pd(OAc)_2$ in a suitable solvent (for example $CHCl_3$, toluene). After stirring for 24 h, the zeolite was separated by centrifugation, and washed twice with the loading solvent (10 ml per g zeolite). The solid was then dried in vacuo (30 °C, 30 mbar, overnight) and used as such.

Reporting Summary. Further information on research design is available in the Nature Research Reporting Summary linked to this article.

Data availability

The findings of this study are available in the main text or the supplementary materials. Atomic coordinates of optimized computational models and initial and final configurations of molecular dynamics trajectories are supplied in a Supplementary Data file. All data are available from the authors upon reasonable request.

Received: 10 January 2020; Accepted: 30 September 2020;
Published online: 16 November 2020

References

1. Hassan, J., Sévignon, M., Gozzi, C., Schulz, E. & Lemaire, M. Aryl–aryl bond formation one century after the discovery of the Ullmann reaction. *Chem. Rev.* **102**, 1359–1469 (2002).
2. Mondschein, R. J. et al. Synthesis and characterization of amorphous bibenzoate (co)polyesters: permeability and rheological performance. *Macromolecules* **50**, 7603–7610 (2017).
3. De Smit, E. et al., Hydroalkylation catalyst and process for use thereof. US patent 2014/0378697 (2014).
4. Dakka, J. M. et al. Biphenyl esters, their production and their use in the manufacture of plasticizers. US patent 9,556,103 (2017).
5. Chen, X., Engle, K. M., Wang, D. -H. & Yu, J. -Q. Palladium(II)-catalyzed C–H activation/C–C cross-coupling reactions: versatility and practicality. *Angew. Chem. Int. Ed.* **48**, 5094–5115 (2009).
6. Xu, B.-Q., Sood, D., Iretskii, A. V. & White, M. G. Direct synthesis of dimethylbiphenyls by toluene coupling in the presence of palladium triflate and triflic acid. *J. Catal.* **187**, 358–366 (1999).
7. Izawa, Y. & Stahl, S. S. Aerobic oxidative coupling of *o*-xylene: discovery of 2-fluoropyridine as a ligand to support selective Pd-catalyzed C–H functionalization. *Adv. Synth. Catal.* **352**, 3223–3229 (2010).
8. Wang, D., Izawa, Y. & Stahl, S. S. Pd-catalyzed aerobic oxidative coupling of arenes: evidence for transmetalation between two Pd(II)–aryl intermediates. *J. Am. Chem. Soc.* **136**, 9914–9917 (2014).
9. Wang, D. & Stahl, S. S. Pd-catalyzed aerobic oxidative biaryl coupling: non-redox cocatalysis by $Cu(OTf)_2$ and discovery of $Fe(OTf)_3$ as a highly effective cocatalyst. *J. Am. Chem. Soc.* **139**, 5704–5707 (2017).
10. Álvarez-Casao, Y. et al. Palladium-catalyzed cross-dehydrogenative coupling of *o*-xylene: evidence of a new rate-limiting step in the search for industrially relevant conditions. *ChemCatChem* **10**, 2620–2626 (2018).
11. Yang, Y., Lan, J. & You, J. Oxidative C–H/C–H coupling reactions between two (hetero)arenes. *Chem. Rev.* **117**, 8787–8863 (2017).
12. Kuhl, N., Hopkinson, M. N., Wencel-Delord, J. & Glorius, F. Beyond directing groups: transition-metal-catalyzed C–H activation of simple arenes. *Angew. Chem. Int. Ed.* **51**, 10236–10254 (2012).
13. Sambiagio, C. et al. A comprehensive overview of directing groups applied in metal-catalysed C–H functionalisation chemistry. *Chem. Soc. Rev.* **47**, 6603–6743 (2018).
14. Leow, D., Li, G., Mei, T.-S. & Yu, J.-Q. Activation of remote *meta*-C–H bonds assisted by an end-on template. *Nature* **486**, 518–522 (2012).
15. Boursalian, G. B., Ham, W. S., Mazzotti, A. R. & Ritter, T. Charge-transfer-directed radical substitution enables *para*-selective C–H functionalization. *Nat. Chem.* **8**, 810–815 (2016).
16. Berger, F. et al. Site-selective and versatile aromatic C–H functionalization by thianthrenation. *Nature* **567**, 223–228 (2019).
17. Dey, A., Maity, S. & Maiti, D. Reaching the south: metal-catalyzed transformation of the aromatic *para*-position. *Chem. Commun.* **52**, 12398–12414 (2016).
18. Van Speybroeck, V. et al. Advances in theory and their application within the field of zeolite chemistry. *Chem. Soc. Rev.* **44**, 7044–7111 (2015).
19. Kosinov, N., Liu, C., Hensen, E. J. M. & Pidko, E. A. Engineering of transition metal catalysts confined in zeolites. *Chem. Mater.* **30**, 3177–3198 (2018).
20. Lawton, S. L., Leonowicz, M. E., Partridge, R. D., Chu, P. & Rubin, M. K. Twelve-ring pockets on the external surface of MCM-22 crystals. *Micropor. Mesopor. Mat.* **23**, 109–117 (1998).
21. Van Velthoven, N. et al. Single-site metal–organic framework catalysts for the oxidative coupling of arenes via C–H/C–H activation. *Chem. Sci.* **10**, 3616–3622 (2019).
22. Kaplan, G. Preparation of biphenols by oxidative coupling of alkylphenols using a recyclable copper catalyst. US patent 2003/0050515 (2003)
23. Eckardt, M., Greb, A. & Simat, T. J. Polyphenylsulfone (PPSU) for baby bottles: a comprehensive assessment on polymer-related non-intentionally added substances (NIAS). *Food Addit. Contam. A* **35**, 1421–1437 (2018).
24. Davies, D. L., Macgregor, S. A. & McMullin, C. L. Computational studies of carboxylate-assisted C–H activation and functionalization at group 8–10 transition metal centers. *Chem. Rev.* **117**, 8649–8709 (2017).
25. Chen, B., Hou, X., Li, Y. & Wu, Y. Mechanistic understanding of the unexpected meta selectivity in copper-catalyzed anilide C–H bond arylation. *J. Am. Chem. Soc.* **133**, 7668–7671 (2011).
26. Deng, C., Zhang, J. & Lin, Z. Theoretical studies on Pd(II)-catalyzed *meta*-selective C–H bond arylation of arenes. *ACS Catal.* **8**, 2498–2507 (2018).
27. Lane, B. S., Brown, M. A. & Sames, D. Direct palladium-catalyzed C-2 and C-3 arylation of indoles: a mechanistic rationale for regioselectivity. *J. Am. Chem. Soc.* **127**, 8050–8057 (2005).

28. Popp, B. V. & Stahl, S. S. Insertion of molecular oxygen into a palladium–hydride bond: computational evidence for two nearly isoenergetic pathways. *J. Am. Chem. Soc.* **129**, 4410–4422 (2007).
29. Konnick, M. & Stahl, S. S. Reaction of molecular oxygen with a Pd^{II}-hydride to produce a Pd^{II}-hydroperoxide: experimental evidence for an HX-reductive-elimination pathway. *J. Am. Chem. Soc.* **130**, 5753–5762 (2008).

Acknowledgements

We thank N. Van Velthoven for discussion. The XAS experiments were performed on beamline BM26A at the European Synchrotron Radiation Facility (ESRF), Grenoble, France. This work was funded by grants from FWO (1S17620N for J.V.; project G0D0518N, G0F2320N, G078118N; EoS BioFACT), the Flemish government (CASAS Methusalem programme for D.D.V.). V.V.S., J.H. and M.B. acknowledge the Research Board of Ghent University (BOF) and funding from the European Union's Horizon 2020 research and innovation programme (consolidator ERC grant agreement No. 647755 – DYNPOR (2015-2020)). The computational resources and services used were provided by Ghent University (Stevin Supercomputer Infrastructure) and the VSC (Flemish Supercomputer Center), funded by the Research Foundation - Flanders (FWO). A.S. and A.B. acknowledge the funding from Russian Science Foundation (joint RSF-FWO grant No. 20-43-01015). A.K. and G.M. acknowledge the financial support from the Slovenian Research Agency (research core funding No. P1-0021 and project No. N1-0079).

Author contributions

Under the supervision of D.D.V., J.V. was responsible for the conception, design and interpretation of the experiments. S.V.M. performed additional experiments. Under the supervision of V.V.S., J.H., S.N. and M.B. performed the DFT calculations. A.B. and A.S. conceived and performed the XAS experiments. A.K. and G.M. conceived and performed the NMR experiments. All authors discussed the results and commented on the manuscript.

Competing interests

J.V., P.T. and D.D.V. filed a patent application GB1804905.6 prior to an international patent application PCT/EP2019/057746.

Additional information

Supplementary information is available for this paper at https://doi.org/10.1038/s41929-020-00533-6.

Correspondence and requests for materials should be addressed to V.V. or D.D.V.

Reprints and permissions information is available at www.nature.com/reprints.

Publisher's note Springer Nature remains neutral with regard to jurisdictional claims in published maps and institutional affiliations.

nature research

Corresponding author(s): Dirk E. De Vos

Last updated by author(s): Sep 14, 2020

Reporting Summary

Nature Research wishes to improve the reproducibility of the work that we publish. This form provides structure for consistency and transparency in reporting. For further information on Nature Research policies, see our Editorial Policies and the Editorial Policy Checklist.

Statistics

For all statistical analyses, confirm that the following items are present in the figure legend, table legend, main text, or Methods section.

n/a	Confirmed
☒	☐ The exact sample size (*n*) for each experimental group/condition, given as a discrete number and unit of measurement
☒	☐ A statement on whether measurements were taken from distinct samples or whether the same sample was measured repeatedly
☒	☐ The statistical test(s) used AND whether they are one- or two-sided *Only common tests should be described solely by name; describe more complex techniques in the Methods section.*
☒	☐ A description of all covariates tested
☒	☐ A description of any assumptions or corrections, such as tests of normality and adjustment for multiple comparisons
☒	☐ A full description of the statistical parameters including central tendency (e.g. means) or other basic estimates (e.g. regression coefficient) AND variation (e.g. standard deviation) or associated estimates of uncertainty (e.g. confidence intervals)
☒	☐ For null hypothesis testing, the test statistic (e.g. *F*, *t*, *r*) with confidence intervals, effect sizes, degrees of freedom and *P* value noted *Give P values as exact values whenever suitable.*
☒	☐ For Bayesian analysis, information on the choice of priors and Markov chain Monte Carlo settings
☒	☐ For hierarchical and complex designs, identification of the appropriate level for tests and full reporting of outcomes
☒	☐ Estimates of effect sizes (e.g. Cohen's *d*, Pearson's *r*), indicating how they were calculated

Our web collection on statistics for biologists contains articles on many of the points above.

Software and code

Policy information about availability of computer code

Data collection

Ab initio molecular dynamics simulations were performed with CP2K 3.0. The static optimization and frequencies calculation of all the periodic transition states and intermediates was done with VASP 5.4.4. The free energy values were then computed starting from the frequency output of VASP using the software TAMkin 1.2.6. Gaussian 09 (revision D.01) was adopted for the optimization and frequencies calculation of the cluster models relative to the active site reoxidation. Frequencies analysis to obtain the Gibbs free energy was in this case done with the GoodVibes code. The minimum-energy crossing points of the reactions involving a change in the spin multiplicity was localized using the MECP code interfaced with Gaussian. State-average vibrational analysis at the MECP was done using the GlowFreq code.
VnmrJ 4.2 (Agilent Technologies) software was used for controlling the Varian NMR spectrometer.
LabSolutions GCsolution software bundle (version 2.44.00) was used for collection of GC-FID data. Agilent MSD ChemStation D.03.00.611 software was used for GC-MS data collection.

Data analysis

VnmrJ 4.2 (Agilent Technologies) software was used for processing the obtained NMR data. SIMPSON 4.2.1 (Aarhus University) software was used for simulating spin dynamics and NMR experiments. MATLAB R2013b (8.2.0.701) (Mathworks) was used for advanced analysis of NMR spectra and preparation of 2D plots. Origin 2018 b9.5.0.193 (academic) (OriginLab Corporation) was used for preparation of 1D plots.
Demeter 0.9.26 (by Bruce Ravel, National Institute of Standards and Technology, USA; Open Source - Artistic License) was used to process raw XAS data and perform first-shell Fourier-Analysis.
ADF 2019.303 (by Software for Chemistry & Materials B.V., Netherlands - Academic group license) was used for calculation of DFT relaxation of geometries for XANES.
FNMNES (by Yves Joly, Institute NEEL CNRS, France – freeware) was used for Ab initio calculation of XANES spectra.
PyFitIt (by the Southern Federal University, Russia; open source (GNU General Public License v3.0)) was used for fitting XANES spectra using ML algorithm.
LabSolutions GCsolution software bundle (version 2.44.00) was used for processing of GC-FID data. MestReNova (Version 12.0.2) was used for analysis of NMR and GC-MS data. Microsoft Office Professional Plus 2016 was used for general processing of catalytic data. PANalytical Data

Viewer (Version 1.8) was used for PXRD processing.

For manuscripts utilizing custom algorithms or software that are central to the research but not yet described in published literature, software must be made available to editors and reviewers. We strongly encourage code deposition in a community repository (e.g. GitHub). See the Nature Research guidelines for submitting code & software for further information.

Data

Policy information about availability of data

All manuscripts must include a data availability statement. This statement should provide the following information, where applicable:

- Accession codes, unique identifiers, or web links for publicly available datasets
- A list of figures that have associated raw data
- A description of any restrictions on data availability

The findings of this study are available in the main text or the supplementary materials. Atomic coordinates of optimized computational models and initial and final configurations of molecular dynamics trajectories are supplied in a Supplementary Data file. All data are available from the authors upon reasonable request.

Field-specific reporting

Please select the one below that is the best fit for your research. If you are not sure, read the appropriate sections before making your selection.

☐ Life sciences ☐ Behavioural & social sciences ☐ Ecological, evolutionary & environmental sciences

For a reference copy of the document with all sections, see nature.com/documents/nr-reporting-summary-flat.pdf

Life sciences study design

All studies must disclose on these points even when the disclosure is negative.

Sample size	*Describe how sample size was determined, detailing any statistical methods used to predetermine sample size OR if no sample-size calculation was performed, describe how sample sizes were chosen and provide a rationale for why these sample sizes are sufficient.*
Data exclusions	*Describe any data exclusions. If no data were excluded from the analyses, state so OR if data were excluded, describe the exclusions and the rationale behind them, indicating whether exclusion criteria were pre-established.*
Replication	*Describe the measures taken to verify the reproducibility of the experimental findings. If all attempts at replication were successful, confirm this OR if there are any findings that were not replicated or cannot be reproduced, note this and describe why.*
Randomization	*Describe how samples/organisms/participants were allocated into experimental groups. If allocation was not random, describe how covariates were controlled OR if this is not relevant to your study, explain why.*
Blinding	*Describe whether the investigators were blinded to group allocation during data collection and/or analysis. If blinding was not possible, describe why OR explain why blinding was not relevant to your study.*

Behavioural & social sciences study design

All studies must disclose on these points even when the disclosure is negative.

Study description	*Briefly describe the study type including whether data are quantitative, qualitative, or mixed-methods (e.g. qualitative cross-sectional, quantitative experimental, mixed-methods case study).*
Research sample	*State the research sample (e.g. Harvard university undergraduates, villagers in rural India) and provide relevant demographic information (e.g. age, sex) and indicate whether the sample is representative. Provide a rationale for the study sample chosen. For studies involving existing datasets, please describe the dataset and source.*
Sampling strategy	*Describe the sampling procedure (e.g. random, snowball, stratified, convenience). Describe the statistical methods that were used to predetermine sample size OR if no sample-size calculation was performed, describe how sample sizes were chosen and provide a rationale for why these sample sizes are sufficient. For qualitative data, please indicate whether data saturation was considered, and what criteria were used to decide that no further sampling was needed.*
Data collection	*Provide details about the data collection procedure, including the instruments or devices used to record the data (e.g. pen and paper, computer, eye tracker, video or audio equipment) whether anyone was present besides the participant(s) and the researcher, and whether the researcher was blind to experimental condition and/or the study hypothesis during data collection.*
Timing	*Indicate the start and stop dates of data collection. If there is a gap between collection periods, state the dates for each sample cohort.*
Data exclusions	*If no data were excluded from the analyses, state so OR if data were excluded, provide the exact number of exclusions and the rationale behind them, indicating whether exclusion criteria were pre-established.*

Non-participation	*State how many participants dropped out/declined participation and the reason(s) given OR provide response rate OR state that no participants dropped out/declined participation.*
Randomization	*If participants were not allocated into experimental groups, state so OR describe how participants were allocated to groups, and if allocation was not random, describe how covariates were controlled.*

Ecological, evolutionary & environmental sciences study design

All studies must disclose on these points even when the disclosure is negative.

Study description	*Briefly describe the study. For quantitative data include treatment factors and interactions, design structure (e.g. factorial, nested, hierarchical), nature and number of experimental units and replicates.*
Research sample	*Describe the research sample (e.g. a group of tagged Passer domesticus, all Stenocereus thurberi within Organ Pipe Cactus National Monument), and provide a rationale for the sample choice. When relevant, describe the organism taxa, source, sex, age range and any manipulations. State what population the sample is meant to represent when applicable. For studies involving existing datasets, describe the data and its source.*
Sampling strategy	*Note the sampling procedure. Describe the statistical methods that were used to predetermine sample size OR if no sample-size calculation was performed, describe how sample sizes were chosen and provide a rationale for why these sample sizes are sufficient.*
Data collection	*Describe the data collection procedure, including who recorded the data and how.*
Timing and spatial scale	*Indicate the start and stop dates of data collection, noting the frequency and periodicity of sampling and providing a rationale for these choices. If there is a gap between collection periods, state the dates for each sample cohort. Specify the spatial scale from which the data are taken*
Data exclusions	*If no data were excluded from the analyses, state so OR if data were excluded, describe the exclusions and the rationale behind them, indicating whether exclusion criteria were pre-established.*
Reproducibility	*Describe the measures taken to verify the reproducibility of experimental findings. For each experiment, note whether any attempts to repeat the experiment failed OR state that all attempts to repeat the experiment were successful.*
Randomization	*Describe how samples/organisms/participants were allocated into groups. If allocation was not random, describe how covariates were controlled. If this is not relevant to your study, explain why.*
Blinding	*Describe the extent of blinding used during data acquisition and analysis. If blinding was not possible, describe why OR explain why blinding was not relevant to your study.*

Did the study involve field work? ☐ Yes ☒ No

Reporting for specific materials, systems and methods

We require information from authors about some types of materials, experimental systems and methods used in many studies. Here, indicate whether each material, system or method listed is relevant to your study. If you are not sure if a list item applies to your research, read the appropriate section before selecting a response.

Materials & experimental systems

n/a	Involved in the study
☒	☐ Antibodies
☒	☐ Eukaryotic cell lines
☒	☐ Palaeontology and archaeology
☒	☐ Animals and other organisms
☒	☐ Human research participants
☒	☐ Clinical data
☒	☐ Dual use research of concern

Methods

n/a	Involved in the study
☒	☐ ChIP-seq
☒	☐ Flow cytometry
☒	☐ MRI-based neuroimaging